Ionics (2015) 21:749–753
DOI 10.1007/s11581-014-1215-z

ORIGINAL PAPER

# The influence of calcium fluoride on the electrochemical dissolution of chalcopyrite in sulfuric acid solution

**Qingyou Liu · Luying Wang · Kai Zheng · Heping Li**

Received: 24 May 2014 / Revised: 28 June 2014 / Accepted: 20 July 2014 / Published online: 2 August 2014


**Abstract** The influence of calcium fluoride on the electrochemical dissolution of chalcopyrite at pH 2 was investigated. Experimental results show, when $CaF_2$ concentration from 0 increased to 10 mg/L, chalcopyrite corrosion current density from 0.316 μA $cm^{-2}$ changed to 0.302 μA $cm^{-2}$, the $CaF_2$ inhibition efficiency is 4.43 % and up to 15.19 % when $CaF_2$ is saturated; electrochemical impedance spectroscopy (EIS) reveals that it is the increase of the charge transfer resistance at the double layer lead to $CaF_2$ restrain chalcopyrite corrosion; and the cause come from copper fluorinated complex formed and are absorbed on the electrode surface.

**Keywords** Chalcopyrite · Calcium fluoride · Polarization curve · EIS · Electrochemical dissolution

## Introduction

Chalcopyrite ($CuFeS_2$) is one of the most abundant primary copper ores and a mineral from which large quantities of copper are extracted. Nicol [15] stated that the interest in the electrochemistry of sulfide minerals is largely due to their ability to dissolve in oxidizing solutions through an electrochemical mechanism. This mechanism is important to hydrometallurgical processes and in the surface activation of sulfide minerals prior to flotation [10]. Therefore, many studies have been dedicated to explaining the dissolution kinetics of chalcopyrite in different media using various electrochemical techniques [1, 18, 24, 27]. Traditionally, the mineral has been treated by smelting technology. Due to the cost-energy efficiencies and the $SO_2$ pollution problem in the process of smelting, a valuable research has been done to obtain a hydrometallurgical process as an alternative choice [7]. Acid leaching is an effective hydrometallurgical process to extract copper, and many researchers have paid their attention on understanding the dissolution properties of chalcopyrite in acid solution. Compared the dissolution of chalcopyrite in water to in acid solution, Deng et al. [5] obtained the result that the lower pH value makes it easier for chalcopyrite to dissolve, and that no matter in water or in acid solution, after long time dissolution, the surface of the chalcopyrite is copper-rich, rough, and increasing lattice imperfections. Some researchers identify the redox reaction products of immobilized chalcopyrite within the potential range of −0.7 to +0.8 V (vs. SCE) in hydrochloric acid solution containing sodium chloride and/or copper (II) chloride by cyclic voltammetry and chronopotentiometry measurements [20].

In nature, fluorite and chalcopyrite are often seen in fluorite-quartz-chalcopyrite mineralization [3, 28, 29]. Fluorite can ionize $F^-$ and thus affects the chalcopyrite hydrometallurgy, especially bio-hydrometallurgical processes. Relevant research has concentrated on fluoride as potentially toxic to bio-hydrometallurgy microorganisms [6, 21, 22, 25] and on the influence of fluoride incorporated into jarosite [9].

In this work, polarization curve and electrochemical impedance spectrum (EIS) were used to investigate the electrochemical dissolution of chalcopyrite in a sulfuric acid solution with varying concentrations of calcium fluoride, with an attempt to discover the effects of calcium fluoride on the chalcopyrite electrochemical dissolution.

Q. Liu · L. Wang · H. Li (✉)
Institute of Geochemistry, Chinese Academy of Sciences,
Guiyang 550002, China
e-mail: liheping123@yahoo.com

L. Wang
University of Chinese Academy of Sciences, Beijing 100039, China

K. Zheng
Hunan Institute of Engineering, Xiangtan 411104, China

## Experimental

### Electrode preparation

Chalcopyrite was obtained from Mt. Lyll, Australia; its chemical composition is listed in Table 1. Chalcopyrite electrode was prepared by cutting the chalcopyrite sample into approximately cubic shape with working areas of 0.20 $cm^2$ and, to the extent possible, no visible imperfections. The specimen was placed on an epoxy resin and was connected to a copper wire using silver paint on the back face, leaving only one face of the electrode exposed to the solution. Prior to each test, the mineral electrode was polished with $1200^{\#}$ carbide paper to obtain a fresh surface, degreased using alcohol, rinsed with deionized water, and dried in a stream of air.

### Electrochemical measurements

Electrochemical measurements were performed using a computer-controlled electrochemical measurement system (PARSTAT 2273, Princeton Applied Research) in a conventional three-electrode electrolytic cell with a platinum auxiliary electrode (AE) and a chalcopyrite working electrode (WE). A saturated calomel electrode (SCE) was used as a reference electrode for all electrochemical tests; all other potentials in this study are quoted with respect to the SCE (0.242 V vs. SHE) if not otherwise stated. The reference electrode was connected to a Luggin capillary to minimize the IR drop. The electrolyte was $H_2SO_4$ (pH 2) with varying concentrations of calcium fluoride: (1) 0 mg/L, (2) 10.0 mg/L, (3) 50.0 mg/L, and (4) saturated. The working, auxiliary and reference electrodes were situated in the same location to ensure a uniform spatial relationship in each experiment. All experiments were conducted at 25±1 °C.

Polarization curve and EIS were utilized to study the chalcopyrite electrode behavior. Polarization curves were obtained by changing the electrode potential automatically from −250 to +250 mV (vs. OCP) at a scan rate of 10 mV $s^{-1}$; the EIS tests were performed at OCP and in the frequency range of 0.001~10,000 Hz with a peak-to-peak amplitude of 10 mV. ZSimpWin 3.20 (2004) software was used to fit the impedance data.

**Table 1** Chemical analysis of the chalcopyrite sample

| Cu, % | Fe, % | S, % | Ca, % | Zn, % | Pb, % | Others, % |
|---|---|---|---|---|---|---|
| 33.7 | 30.8 | 34.2 | <0.01 | <0.01 | <0.10 | 1.3 |

## Results and discussion

### Polarization curve study

As is well known, chalcopyrite belongs to semiconductor, so depending on polarization curve study, we can figure out the influences of calcium fluorides of different concentration on the electrochemical dissolution of chalcopyrite. The polarization curve for the chalcopyrite electrode in sulfuric acid solution (pH 2) with different concentrations of calcium fluoride is provided in Fig. 1.

The cathodic branch of polarization curves given rise to parallel lines with increasing $CaF_2$ concentration, while cathodic corrosion current density decreased slowly, revealing that the addition of $CaF_2$ does not change the cathodic oxygen redox mechanism and the decrease of $O_2$ on cathodic surface mainly through a charge transfer mechanism. The suppression of cathodic process can be attributed to the decreasing of the quantity of available oxygen as Moslemi et al. stated [14].

For the anodic part of polarization curves, when electrolyte without $CaF_2$, at the polarization initial stage, the anodic corrosion current densities increase dramatically and the anodic is in the region of strong polarization, with the polarization potentials change positively, the anodic corrosion current densities are still increased, but the increase rate changes very slowly, especially at the potential region of ~50 to ~150 mV, and then, higher positive potentials cause the anodic corrosion current densities obviously increase again. When electrolyte has $CaF_2$, at the polarization initial stage, bigger concentrations of $CaF_2$ increase the anodic corrosion current densities, when potential change more positively, this trend will inverse, that is, more $CaF_2$ resulting in smaller anodic corrosion current densities.

The explanations for the abovementioned data are shown in the following: the chalcopyrite electrochemical reactions at

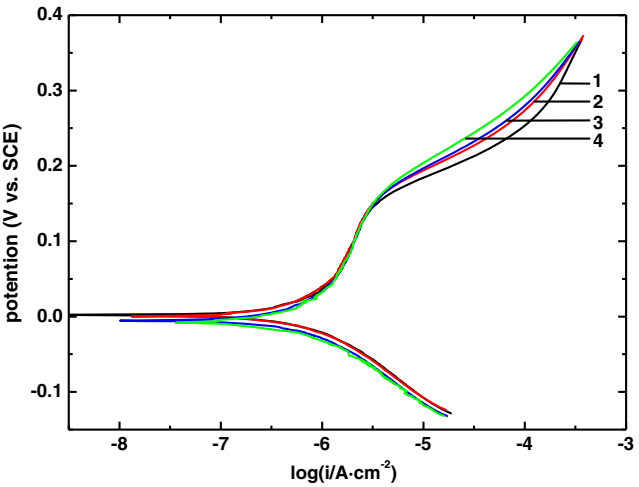


**Fig. 1** Potentiodynamic curves of the chalcopyrite electrode. Conditions: 298 K, $C_{CaF_2}$ (*1*) 0; (*2*) 10.0; (*3*) 50.0 mg/L; and (*4*) saturated

**Table 2** Electrochemical parameters of $CuFeS_2$

| $CaF_2$ (mg $L^{-1}$) | $E_{corr}$ (mV) | $i_{corr}$ (μA $cm^{-2}$) | $\eta$ (%) | $b_c$ (mV) | $b_a$ (mV) |
|---|---|---|---|---|---|
| 0 | 2.2 | 0.316 | | 133.4 | 525.2 |
| 10 | 1.6 | 0.302 | 4.43 | 131.2 | 513.1 |
| 50 | −4.7 | 0.288 | 8.86 | 129.1 | 471.5 |
| saturated | −7.2 | 0.268 | 15.19 | 123.4 | 447.8 |

the anode and cathode are shown in Eqs. (1) and (2) as reported by Koleini et al. [12] and Klauber [11]. Reaction (1) shows chalcopyrite was oxidized to $Cu^{2+}$, $Fe^{2+}$, and $S^0$ in the sulfuric acid solution, with the anodic potential scan to positive, more $S^0$ formed and thus caused the anodic corrosion current densities increase the rate change slowly. When electrolyte has $CaF_2$, $F^-$, and $Cu^{2+}$ form fluorinated complex (reactions 3–6) according to the report of Connick and Paul [4], which prompting chalcopyrite anodic reaction, resulting anodic corrosion current densities change bigger; however, with potentials scan to positive, more fluorinated complex were formed and adsorbed on the electrode surface, restraining chalcopyrite electrochemical dissolution.

Anodic reaction:

$$CuFeS_2 \rightarrow Cu^{2+} + Fe^{2+} + 2S^0 + 4e^- \quad (1)$$

Cathodic reaction:

$$O_2 + 4H^+ + 4e^- = 2H_2O \quad (2)$$

Complex reactions:

$$Cu^{2+} + HF = CuF^+ + H^+ \quad (3)$$

$$Cu^{2+} + F^- = CuF^+ \quad (4)$$

$$Cu^{2+} + 2F^- = CuF_2 \quad (5)$$

$$Cu^{2+} + nF^- = CuF_n^{(n-2)-} (n = 3, 4, 6) \quad (6)$$

Table 2 collects the associated corrosion electrochemical parameters of chalcopyrite, respectively, such as corrosion potential ($E_{corr}$), corrosion current density ($i_{corr}$), Tafel slopes of cathode ($b_c$), and anode ($b_a$) derived from polarization curves by extrapolation, as well as the percentage inhibition efficiency

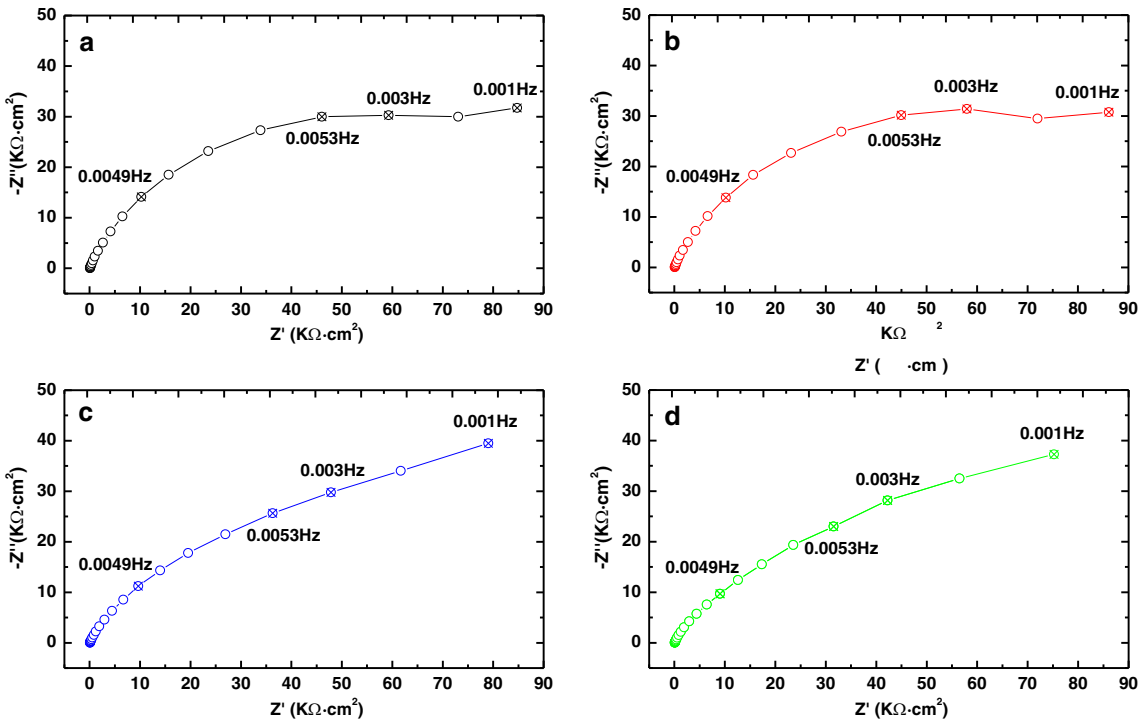


**Fig. 2** Nyquist plots of the chalcopyrite electrode at OCP. Conditions: 298 K, $C_{CaF_2}$ (1) 0; (2) 10.0; (3) 50.0 mg/L; and (4) saturated

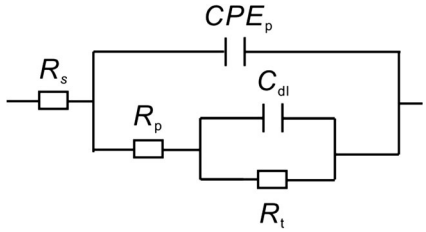


**Fig. 3** Equivalent circuit for the chalcopyrite electrode/electrolyte at OCP

($\eta$). Here, the $\eta$ is defined by following equation, which is often used in material science [23, 26]:

$$\eta\,\% = \frac{i^0_{\mathrm{corr}} - i_{\mathrm{corr}}}{i^0_{\mathrm{corr}}} \times 100 \tag{8}$$

where $i^0_{\mathrm{corr}}$ and $i_{\mathrm{corr}}$ are the corrosion current densities when electrolyte is without and with $CaF_2$, respectively. It is evident that increasing concentration of $CaF_2$ resulted in a decrease in corrosion current densities and an increase in $\eta$%, suggesting that the adsorption protective fluorinated complex $CuF_n^{(n-2)-}$ ($n$=3, 4, 6) tends to be more complete and stable on electrode surface. The presence of $CaF_2$ resulted in a slight shift of corrosion potential toward the negative direction and further negative with increasing concentration of $CaF_2$ through control of anodic reaction. Moreover, the values of the anodic and cathodic Tafel slopes show no obvious changes with the addition of $CaF_2$, confirming that it impede by merely blocking the reaction sites of electrode surface without affecting the anodic and cathodic reaction mechanism. These results are in good agreement with the conclusion that $F^-$ ions are only complex with $Cu^{2+}$ while not participating in electrode reaction.

## Electrochemical impedance spectroscopy study

Electrochemical impedance spectroscopy has been widely applied to study the characteristics of electrodes and electrochemical reactions [16]. All EIS data were fitted to equivalent electrochemical circuits (EEC) using a nonlinear method [2]. The equivalent circuits represent an approach to describing the electrochemical processes that take place at the electrode/electrolyte interface, and any models derived from these circuits are only speculative [13]. Therefore, different EECs were used to fit the EIS data, and only those results with the best fitting values capable of efficiently explaining the electrode/electrolyte interface were reported.

Figure 2 presents the Nyquist plots for chalcopyrite in different concentrations of $CaF_2$. The Nyquist plots are composed of two capacitive loops; the one at high frequencies is attributed to the charge transfer resistance ($R_t$), which could correspond to the resistance between the chalcopyrite and the outer Helmholtz plane; the other slightly distorted capacitive loop at low frequencies is related to the combination of a pseudo-capacitance impedance (due to the passive layer) and a resistance $R_p$. The deviation from an ideal semicircle is generally attributed to the frequency dispersion as well as to the inhomogeneities of the passive layer surface. The related electrochemical equivalent circuit used to model the chalcopyrite/electrolyte interface is shown in Fig. 3, where $R_s$ is the electrolyte and other ohmic resistance, $R_t$ is the charge transfer resistance, $R_p$ is the film resistance, $C_{dl}$ is the double layer capacitance, $CPE_p$ represent constant phase element to replace the passive film capacitance ($C_p$), and $n$ shows the phase shift which can be explained as the degree of surface inhomogeneity [17].

The impedance parameters obtained by fitting the EIS data to the equivalent circuit are listed in Table 3. Charge transfer resistance $R_t$ reveal that $CaF_2$ inhibited chalcopyrite electrochemical reaction. It is apparent from Table 3 that by increasing concentration of $CaF_2$, the double-layer capacitance $C_{dl}$ or $CPE_{dl}$, $Y_0$ values tended to decrease, the $R_t$ values increased. This decrease in the $C_{dl}$ or $CPE_{dl}$, $Y_0$ can be attributed to the decrease in local dielectric constant and/or an increase in the thickness of the electrical double layer, suggesting that fluorinated complex formed and adsorbed at the interface of electrode/solution. The increases in the $R_t$ value indicate that the amount of fluorinated complex adsorbed on the electrode surface and consequently become a barrier to hinder the mass and charge transfer, resulting in an increase in the inhibition efficiency. These results are in good agreement with those from polarization results.

The passive film capacitance $CPE_p$, $Y_0$ values increased and the $R_p$ values decreased with increasing concentration of $CaF_2$. These results are attribute to $F^-$ ions penetrate the passive film and reach the electrode surface, preventing or postponing the neutralization of the surface, which is often seen in halogen ions [19]. Two causes are attribute to $F^-$ ions' penetrate process; firstly, $F^-$ ion has very small ionic radius and therefore has strong penetration; secondly, as the oxidized

**Table 3** Model parameters for equivalent circuit of Fig. 2

| $CaF_2$ (mg $L^{-1}$) | $C_{dl}$ (F $cm^{-2}$) | $R_t$ ($\Omega$ $cm^2$) | $CPE_p$, $Y_0$ (S $cm^{-2}$ $s^{-n}$) | $n$ | $R_p$ ($\Omega$ $cm^2$) |
|---|---|---|---|---|---|
| 0 | $1.320\times10^{-3}$ | $3.510\times10^{4}$ | $1.189\times10^{-4}$ | 0.7680 | $6.780\times10^{4}$ |
| 10 | $1.161\times10^{-3}$ | $3.631\times10^{4}$ | $1.191\times10^{-4}$ | 0.7604 | $6.663\times10^{4}$ |
| 50 | $1.046\times10^{-3}$ | $5.559\times10^{4}$ | $1.245\times10^{-4}$ | 0.7246 | $5.253\times10^{4}$ |
| Saturated | $8.747\times10^{-4}$ | $5.944\times10^{4}$ | $1.289\times10^{-4}$ | 0.7220 | $3.999\times10^{4}$ |

product, most of the sulfur could be on the chalcopyrite. However, the SEM indicates that the elemental sulfur exhibits porous structure and it does not completely block the ion/water transport/diffusion to or from the surface [8, 18]. The exponent $n$ values decreased, confirming that the degree of passive surface inhomogeneity increased with increasing concentration of $CaF_2$.

## Conclusions

The presence of $CaF_2$ raises to the reduction in the quantity of available oxygen and the formation of the fluorinated complex $CuF_n^{(n-2)-}$ ($n$=3, 4, 6), resulting in inhibit chalcopyrite electrochemical dissolution. When electrolyte contained 10 mg/L $CaF_2$, the inhibition efficiency is 4.43 % and up to 15.19 % when $CaF_2$ is saturated and this phenomenon attribute to fluorinated complex adsorbed on the electrode surface and consequently become a barrier to hinder the mass and charge transfer, though $F^-$ ions can penetrate the passive film.

**Acknowledgments** This work was financially supported by the 135 Program of the Institute of Geochemistry, CAS, the National Natural Science Foundation of China (40803017), and by the Key Technologies R & D Program of Guizhou Province, China (SY[2011]3088).

## References

1. Biegler T, Swift D (1979) Anodic electrochemistry of chalcopyrite. J Appl Electrochem 9(5):545–554
2. Boukamp BA (1986) A nonlinear least squares fit procedure for analysis of immittance data of electrochemical systems. Solid State Ionics 20(1):31–44
3. Chang Z, Meinert LD (2008) The Empire Cu-Zn Mine, Idaho: exploration implications of unusual skarn features related to high fluorine activity. Econ Geol 103(5):909–938
4. Connick RE, Paul AD (1958) The Fluoride complexes of zinc, copper and lead ions in aqueous solution. J Am Chem Soc 80(9):2069–2071
5. Deng JS et al (2012) Spectroscopic Characterization of dissolubility and surface properties of chalcopyrite in aqueous solution. Spectrosc Spectr Anal 32(2):519–524
6. Dopson M et al (2008) Silicate mineral dissolution during heap bioleaching. Biotechnol Bioeng 99(4):811–820
7. Dutrizac JE (1978) Kinetics of dissolution of chalcopyrite in ferric ion media. Metallurgical Transactions B-process Metallurgy 9(3):431–439
8. Elsherief A (2002) The influence of cathodic reduction, $Fe^{2+}$ and $Cu^{2+}$ ions on the electrochemical dissolution of chalcopyrite in acidic solution. Miner Eng 15(4):215–223
9. Gunneriusson L et al (2009) Jarosite inclusion of fluoride and its potential significance to bioleaching of sulphide minerals. Hydrometallurgy 96(1):108–116
10. Holliday R, Richmond W (1990) An electrochemical study of the oxidation of chalcopyrite in acidic solution. Journal of Electroanalytical Chemistry and Interfacial Electrochemistry 288(1):83–98
11. Klauber C (2008) A critical review of the surface chemistry of acidic ferric sulphate dissolution of chalcopyrite with regards to hindered dissolution. Int J Miner Process 86(1–4):1–17
12. Koleini S, Aghazadeh V, Sandstrom A (2011) Acidic sulphate leaching of chalcopyrite concentrates in presence of pyrite. Miner Eng 24(5):381–386
13. Macdonald JR (1985) Generalizations of "universal dielectric response"and a general distribution–of–activation–energies model for dielectric and conducting systems. J Appl Phys 58(5):1971–1978
14. Moslemi H, Shamsi P, Habashi F (2011) Pyrite and pyrrhotite open circuit potentials study: effects on flotation. Miner Eng 24(10):1038–1045
15. Nicol MJ (1984) An electrochemical study of the interaction of copper (II) ions with sulphide minerals. Electrochemistry in mineral and metal processing. In: Richardson PE, Srinivasan S, Woods R (eds) The Electrochemical Society. Pennington, New Jersey, 152–166 pp
16. Orazem ME, Tribollet B (2008) Electrochemical impedance spectroscopy, 2nd edn. John wiley& Sons, Inc., Hoboken, New Jersey, 38 pp
17. Ozcan M, Karadag F, Dehri I (2008) Investigation of adsorption characteristics of methionine at mild steel/sulfuric acid interface: an experimental and theoretical study. Colloids Surf A Physicochem Eng Asp 316(1):55–61
18. Parker A, Paul R, Power G (1981) Electrochemistry of the oxidative leaching of copper from chalcopyrite. Journal of Electroanalytical Chemistry and Interfacial Electrochemistry 118:305–316
19. Pavlica JJ (1974) Electrochemistry of pyrrhotite in flotation, University of Minnesota
20. Pikna L, Lux L, Grygar T (2006) Electrochemical dissolution of chalcopyrite studied by voltammetry of immobilized microparticles. Chemical Papers-Chemicke Zvesti 60(4):293–296
21. Schippers A, Von Rege H, Sand W (1996) Impact of microbial diversity a sulfur chemistry on safeguarding sulfudic mine waste. Miner Eng 9(10):1069–1079
22. Sicupira L, Veloso T, Reis F, Leao V (2011) Assessing metal recovery from low-grade copper ores containing fluoride. Hydrometallurgy 109(3):202–210
23. Solmaz R, Kardaş G, Yazıcı B, Erbil M (2008) Adsorption and corrosion inhibitive properties of 2-amino-5-mercapto-1, 3, 4-thiadiazole on mild steel in hydrochloric acid media. Colloids Surf A Physicochem Eng Asp 312(1):7–17
24. Stankovic Z (1986) The anodic dissolution reaction of chalcopyrite. Erzmetall 39(12):623–628
25. Suzuki I, Lee D, Mackay B, Harahuc L, Oh JK (1999) Effect of various ions, pH, and osmotic pressure on oxidation of elemental sulfur by *Thiobacillus thiooxidans*. Appl Environ Microbiol 65(11):5163–5168
26. Wang X, Yang H, Wang F (2011) An investigation of benzimidazole derivative as corrosion inhibitor for mild steel in different concentration HCl solutions. Corros Sci 53(1):113–121
27. Warren G, Wadsworth M, El-Raghy S (1982) Passive and transpassive anodic behavior of chalcopyrite in acid solutions. Metall Trans B 13(4):571–579
28. Young B (1996) Bismuth-beating assemblages from the Northern Pennine Orefield. Mineral Mag 60:317–324
29. Zhai D et al (2014) Zircon U–Pb and molybdenite Re–Os geochronology, and whole-rock geochemistry of the Hashitu molybdenum deposit and host granitoids, Inner Mongolia, NE China. J Asian Earth Sci 79:144–160